Infrared Spectra and Density Functional Calculations for $M(OH)_{2,3}$ and HOMO Molecules and $M(OH)_2^+$ Cations (M = Y, La)

Xuefeng Wang and Lester Andrews*

Department of Chemistry, University of Virginia, McCormick Road, P.O. Box 400319, Charlottesville, Virginia 22904-4319

Received: December 2, 2005; In Final Form: February 3, 2006

Reactions of laser-ablated Y and La atoms with H_2O_2 gives the $M(OH)_2$ and $M(OH)_3$ molecules and the HOMO dehydration product, and the cation $M(OH)_2^+$ in solid argon. Density functional calculations show that the dihydroxide molecules and cations are bent at the metal center, and the symmetric and antisymmetric O−H stretching modes are both observed in the infrared spectra. The trihydroxide molecules have calculated C_{3h} structures characterized by strong antisymmetric O−H and M−O stretching modes. Mulliken charges increase for all product molecules going down the Group 3 family and increase as one, two, and three OH ligands are bonded to the metal center. Evidence is also presented for the $Y(OH)_4^-$ anion.

Introduction

The Group 3 metals form ionic crystalline trihydroxide $M(OH)_3$ solids, which have been characterized by X-ray and neutron diffraction methods.[1−7] Group 3 trihydroxides are not nearly as common as the Group 2 dihydroxides, but in contrast pure Group 4 hydroxides appear to be unknown although structures of the mixed $Zr(OH)_2SO_4$ and $Hf(OH)_2SO_4$ salts have been determined.[6−10]

The YOH molecule has been observed by high-resolution electronic spectroscopy in the gas phase, and the linear structure and frequencies have been measured.[11] Group 3 metal atom reactions with water molecules have been investigated by two research groups using matrix isolation methods. The first employed thermal Sc atoms and photochemistry and the second used laser-ablated Sc.[12,13] The Fudan workers also investigated Y and La reactions, and assigned new metal−oxide stretching absorptions to $Y(OH)_2$, $La(OH)_2$, and other products, but they did not analyze the O−H stretching region because of strong water precursor absorptions.[14] Very recently Sc atoms have been reacted with H_2O_2 in this laboratory, and the $Sc(OH)_2$, $Sc(OH)_3$, and HOScO molecules and $Sc(OH)_2^+$ cation identified from both O−H and Sc−O stretching modes.[15] Gas-phase reactions have been investigated, and the thermochemistry of $Sc(OH)_n^+$ cation dissociation considered by several groups.[16−18] Calculations of successive OH binding energies to M^+ cations have been performed for first row transition metal $M(OH)_n^+$ cations.[19,20]

Experimental and Theoretical Methods

Laser-ablated Y and La metal atoms were reacted with hydrogen peroxide and hydrogen/oxygen mixtures during codeposition in excess argon as described for previous investigations with oxygen and hydrogen.[21−25] A urea−hydrogen peroxide complex (Aldrich) was placed in the sidearm of a Chemglass valve, and argon was passed through this apparatus at 3 mmol/h to entrain H_2O_2 vapor as employed for Group 2, 4, and 12 reactions.[26−28] Deuterium enriched (90%) peroxide was prepared by using previous work as a guide.[29,30] A Nd:YAG laser was focused (10 cm f.l.) onto the rotating metal target (5−40 mJ/pulse, 10 Hz) about 2 cm from the 12 K cesium iodide sample collecting window. Infrared spectra were measured on a Nicolet 750 spectrometer after sample deposition, after sample warming to allow diffusion, and after irradiation by a mercury arc street lamp. Similar experiments were performed with hydrogen and oxygen isotopic mixtures.

Quantum chemical calculations of structures and vibrational frequencies were done for anticipated product molecules, using the Gaussian 98 program system, the B3LYP density functional, 6-311++G(3df,3pd) basis set for H and O, and the SDD pseudopotential and basis for Y and La atoms.[31−33] Gaussian NBO Version 3.1 was used to compute natural electron configurations. All structural parameters were varied, and the converged minima are stable structures with real frequencies.

Results

Infrared spectra and density functional calculations of Y and La metal atom−hydrogen peroxide and hydrogen/oxygen reaction products will be presented. Absorptions common to laser-ablation experiments due to the H_2O−HO radical complex and HO_2 and OH radicals were also observed.[34−36]

Yittrium. The Y reaction gave the highest Group 3 product yield in part because this hard metal with a regular surface laser-ablates more efficiently. Figure 1 illustrates the spectrum of Y + H_2O_2 reaction products, and Table 1 lists the observed frequencies. Strong bands at 3785.1 cm^{-1} (labeled **tri**) and at 3772.7 cm^{-1} (labeled **di**) and weaker bands at 3736.8, 3734.2 cm^{-1} (labeled **dic**) and at 3778.7 cm^{-1} (labeled **h**) are observed in the O−H stretching region, and weak YO^+, YO, and HYO bands at 871.6, 843.2, and 809.6 cm^{-1}, respectively,[14,22] and a stronger 788.2 cm^{-1} band (labeled HOYO), 680.2 and 662.2 cm^{-1} absorptions (labeled **dic**), medium intensity 616.9, 598.0, and 592.7 cm^{-1} bands (labeled **h**, **di**, and **tri**), a weaker 550.5 cm^{-1} band (labeled HOYO) and a final weak 459 cm^{-1} absorption (labeled **a**) are observed in the Y−O stretching region on sample deposition. Absorptions due to H_2O_2 and its photolysis product HOH−O complex (labeled **c**) and water (labeled **w**) were also observed.[26−30] Annealing to 20 K slightly increased the **di** and **tri** bands and sharpened the other absorptions. The

* Address correspondence to this author. E-mail: lsa@virginia.edu.

10.1021/jp0570263 CCC: $33.50
Published on Web 03/07/2006

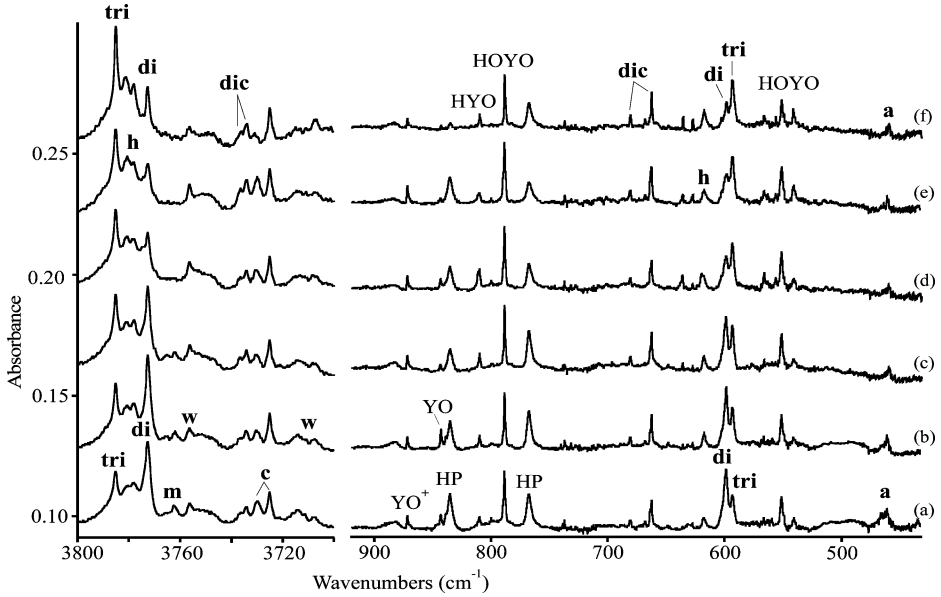

Figure 1. Infrared spectra in the O−H and Y−O stretching regions for laser-ablated Y atom and H_2O_2 reaction products in excess argon at 10 K: (a) Y and H_2O_2 co-deposited for 60 min, (b) after annealing to 20 K, (c) after >320 nm irradiation, (d) after 240−380 nm irradiation, (e) after >220 nm irradiation, and (f) after annealing to 28 K.

TABLE 1: Infrared Absorptions (cm^{-1}) for Products of the Reaction of Y Atoms and H_2O_2 or $H_2 + O_2$ Molecules

$H_2O_2/H_2 + O_2$	$D_2O_2/D_2 + O_2$	$H_2 + {}^{18}O_2$	$HD + O_2$	$D_2 + {}^{18}O_2$	identification
3785.1/3785.2	2793.0	3773.5	3785.5, 2793.4	2774.0	**tri**, $Y(OH)_3$
/3778.8	2790.6	3766.8		2770.8	**h**, $HY(OH)_2$
	2785.8/2785.8			2768.0	**di**, $Y(OH)_2$
3772.7/3773.1	2783.9/2784.0	3761.1	3773.5, 2784.9	2766.5	**di**, $Y(OH)_2$
3762.1	2778.5				**m**, (YOH)
3736.8/3737.0	2759.7/2759.6				**dic**, $Y(OH)_2^+$
3734.2/3734.3	2755.6/2755.5	3722.3	3773.5, 2784.9	2738.3	**dic**, $Y(OH)_2^+$
/1368.7	980.8	1368.7		980.7	**h**, $HY(OH)_2$
809.7	807.9				HYO
788.2/788.6	788.0/788.3	750.5	788.5	750.3	HOYO
680.5	667.7	648.6			**dic**, $Y(OH)_2^+$
662.2	651.3	634.9	655.0	626.2	**dic**, $Y(OH)_2^+$
616.9/617.5	592.6/592.3	599.7	616, 610, 593	571.9	**h**, $HY(OH)_2$
598.0/598.6	596.2/596.7	575.8	598.6	574.1	**di**, $Y(OH)_2$
592.7/592.5	577.8/577.9	556.3	577	570.4	**tri**, $Y(OH)_3$
550.5/550.5	537.6/538	527.6	538.6		HOYO
459	442				**a**, $Y(OH)_4^-$

irradiation sequence >320 nm, 240−380 nm, >220 nm decreased the **di** and increased the **tri** bands, and the final >220 nm irradiation also increased the **dic** and reduced the **h** bands (Figure 1). A final annealing to 28 K slightly increased the **tri**, **h**, and **di** bands.

Similar experiments with lower laser energies gave weaker product absorptions, and the **di** bands were favored over the **tri** absorptions and the **h** bands were not observed with comparable low hydrogen peroxide concentrations. At higher hydrogen peroxide levels the **tri** bands were stronger than the **di** absorptions, and the **dic** bands were twice as intense as shown in the Figure 1 spectra.

One experiment was done by codepositing Ar/H_2O_2 and Ar/CCl_4 (0.2%) with Y atoms under the same laser-ablation and hydrogen peroxide conditions employed in the sample for Figure 1. The effect of the chlorocarbon in competition for the Y reagent is to reduce the original product yield, in this case by about a factor of 3, without altering the **di** to **tri** product ratio, to increase the **dic** band intensities relative to **di** by a factor of 4, and to double the YO^+ band relative to YO. Ultraviolet irradiation served to further increase the yield of **dic** relative to **di** and YO^+ relative to YO, as shown in the spectra of Figure 2.

The Y atom reaction with D_2O_2 was also investigated, and the spectra are illustrated in Figure 3. The O−D stretching region contains new bands at 2793.0 cm^{-1} (labeled **tri**), a doublet at 2785.3, 2783.8 cm^{-1} (labeled **di**), a 2778.5 cm^{-1} band (labeled **m**), and a doublet at 2759.7, 2755.6 cm^{-1} (labeled **dic**). Annealing improved resolution of the two doublets, and UV irradiation reduced the **di** bands in favor of the **tri** bands and slightly increased the **dic** bands. Associated bands in the Y−O stretching region exhibit common behavior on annealing and irradiation (Table 1).

Infrared spectra of like stoichiometry $Y + H_2 + O_2$ reaction products are compared in Figure 4. Many of the same absorptions are observed, but the relative intensities are different from the reaction with hydrogen peroxide. First weak yittrium oxide bands and stronger yittrium hydride species are observed. Second, the 1368.7 and 616.9 cm^{-1} bands are much stronger and a new associated 3778.7 cm^{-1} band (labeled **h**) is observed in the O−H stretching region. Third, the **dic** bands are slightly weaker. Fourth, the **di** bands are slightly shifted to 3773.1 and 598.6 cm^{-1}, and they are stronger, but they exhibit the same annealing and irradiation behavior as with H_2O_2 and give way to the **tri** bands as before. Figure 5 shows the effect of isotopic substitution in the hydrogen and oxygen reagents, and the band

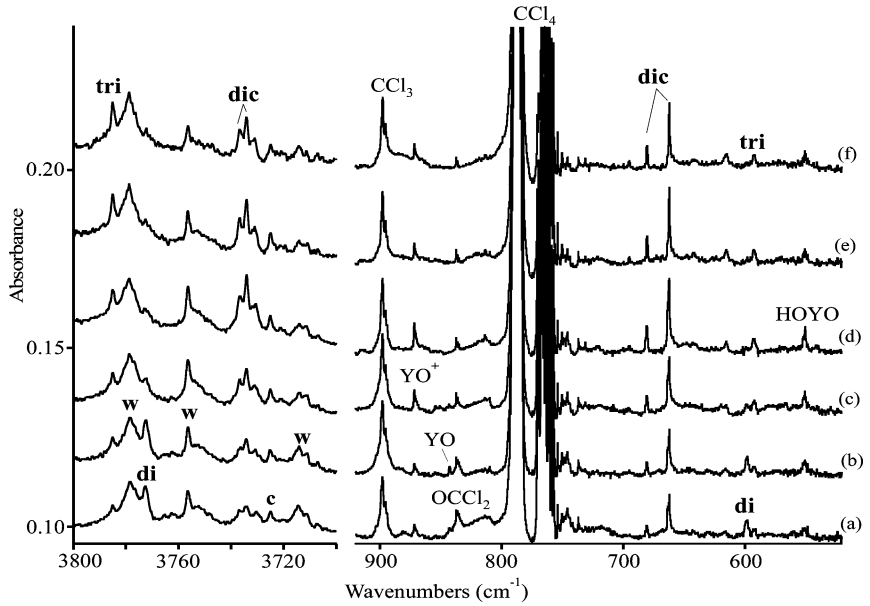

Figure 2. Infrared spectra in the O−H and Y−O stretching regions for laser-ablated Y atom and H_2O_2 reaction products in solid argon containing approximately 0.1% CCl_4: (a) Y, H_2O_2, and CCl_4 co-deposited for 60 min, (b) after annealing to 20 K, (c) after >320 nm irradiation, (d) after 240−380 nm irradiation, (e) after >220 nm irradiation, and (f) after annealing to 28 K.

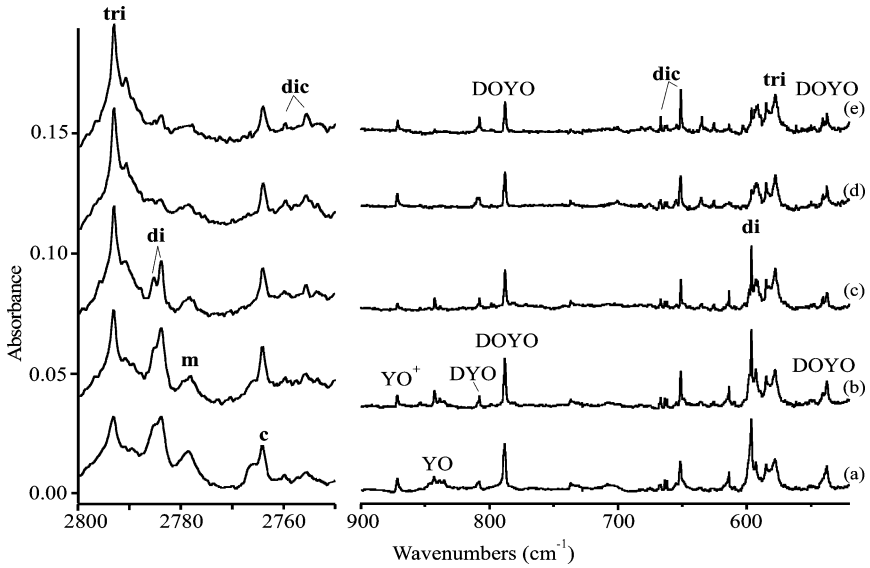

Figure 3. Infrared spectra in the O−D and Y−O stretching regions for laser-ablated Y atom and D_2O_2 reaction products in excess argon at 10 K: (a) Y and D_2O_2 co-deposited for 60 min, (b) after annealing to 20 K, (c) after annealing to 26 K, (d) after 240−380 nm irradiation, and (e) after annealing to 28 K.

positions are also listed in Table 1. The HD reagent results in small diagnostic shifts in the O−H and O−D stretching regions. Two experiments with $^{16}O_2$, $^{16}O^{18}O$, $^{18}O_2$ sample gave broad doublet absorptions at 3773, 3761 cm^{-1} and 599, 575 cm^{-1} for the **di** bands, and at 3785, 3773 cm^{-1} for the **tri** absorptions.

The 3700 cm^{-1} region of the Y-water reaction product spectrum of the Fudan group[14] was examined for bands common to the present experiments. Weak new bands were observed at 3785.1, 3772.6, 3735.9, and 3737.6 cm^{-1} and they track on annealing with lower frequency bands at 592.8, 597.9, and 662.2 cm^{-1}, respectively.

Calculations were done at the B3LYP level for the products anticipated from the analogous scandium reactions,[15] and the harmonic (unscaled) frequencies are listed in Tables 2−5 and the structures are illustrated in Figure 6. In addition to $Y(OH)_2$, calculations were also done for $Y(OH)_2^+$ cation and $Y(OH)_2^-$ anion. The cation is 136 kcal/mol higher and the anion 19 kcal/mol lower in energy than the molecule. The anion has low infrared intensities, and it would be difficult to detect in these experiments based on the three highest calculated frequencies 3970 (b_2, 13 km/mol), 3968 (a_1, 15 km/mol), and 565 cm^{-1} (b_2, 43 km/mol). However, the $Y(OH)_4^-$ anion is very stable, analogous to YH_4^-, and it has an S_4 structure and a very strong degenerate Y−O stretching mode calculated at 502 cm^{-1} (404 km/mol) and a weak degenerate O−H stretching mode calculated at 3939 cm^{-1} (42 km/mol).

Lanthanum. Analogous experiments were performed with the softer metal lanthanum, which does not give as high an ablation yield as yittrium. Laser-ablated lanthanum atoms were reacted with H_2O_2 using two laser energies and sample concentrations. The initial deposit shows weak new bands at 3740.6, 3730.3, 3693.2, and 3690.9 cm^{-1} (labeled, **tri**, **di**, and **dic**, respectively) in the O−H stretching region and new bands at 742.5 and 480.6 cm^{-1} (labeled HOLaO), at 624.2 and 580.3 cm^{-1} (labeled **dic**), at 519.5 cm^{-1} (labeled **di**), and at 507.5 and 491.4 cm^{-1} (labeled **tri**) in the La−O stretching region

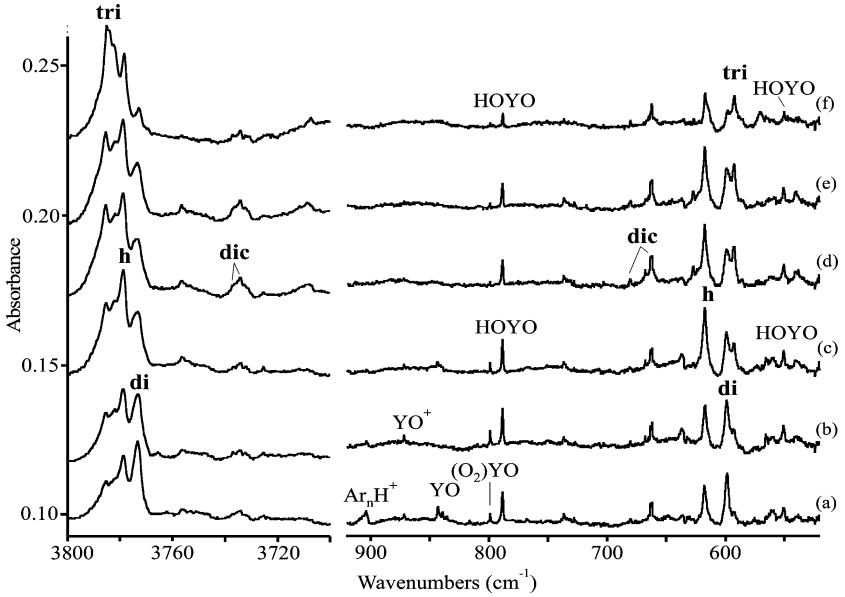

Figure 4. Infrared spectra in the O−H and Y−O stretching regions for laser-ablated Y atom and H_2 plus O_2 reaction products in excess argon at 10 K: (a) Y and H_2 (6%) plus O_2 (0.4%) co-deposited for 60 min, (b) after >320 nm irradiation, (c) after 240−380 nm irradiation, (d) after >220 nm irradiation, (e) after annealing to 14 K, and (f) after annealing to 28 K.

TABLE 2: Observed and Calculated Frequencies (cm^{-1}) for $Y(OH)_2$ in the C_{2v} Structure $^2A_1$ Ground State

	$Y(OH)_2$		$Y(OH)(OD)$		$Y(OD)_2$		$Y(^{18}OH)_2$		$Y(^{18}OD)_2$	
mode	obsd[a]	calcd[b]	obsd	calcd	obsd	calcd	obsd	calcd	obsd	calcd
O−H stretch		3965.5 (a_1, 110)[c]	3773.5	3963.3 (177)	2785.8	2891.1 (77)	3770.4	3952.1 (106)	2768.0	2870.9 (101)
O−H stretch	3773.1	3964.9 (b_2, 158)	2784.9	2889.0 (130)	2784.0	2889.7 (123)	3761.1	3951.5 (149)	2766.5	2968.9 (139)
Y−O stretch	598.6	625.7 (a_1, 224)	598.4	723.0 (227)	596.7	608.5 (176)	575.8	598.7 (148)	574.1	692.5 (220)
Y−O stretch		624.2 (a_1, 165)		670.5 (90)		607.8 (45)		595.5 (55)		633.9 (73)
Y−O−H bend		386.7 (a_2, 0)		354.6 (101)		288.3 (55)		384.3 (0)		280.2 (49)
Y−O−H bend		377.2 (b_1, 171)		344.7 (88)		288.2 (0)		373.9 (168)		258.9 (0)
Y−O−H bend		375.4 (a_1, 85)		269.2 (68)		287.8 (98)		371.7 (81)		257.8 (105)
Y−O−H bend		335.4 (b_2, 130)		262.0 (59)		251.6 (69)		333.0 (130)		252.8 (70)
O−Y−O bend		113.6 (a_1, 1)		110.9 (0)		105.3 (0)		109.2 (1)		103.5 (0)

[a] Observed **di** bands in solid argon. [b] Calculated at the B3LYP/6-311++G(3df,3pd)/SDD level. [c] Mode symmetry in C_{2v}, infrared intensity, km/mol.

(Figure 7). Ultraviolet irradiation (240−380 nm) decreased the **di** bands and increased the others, and the full arc (>220 nm) continued this trend plus formed the HOH−O complex (labeled **c**). Subsequent annealing to 26 K increased the **tri** and decreased the other bands, and a final full-arc irradiation sharpened the **tri** bands. Higher laser energy gave a higher product yield, particularly **tri** and the HOH−O complex on sample deposition.

Complementary reactions were also done with H_2 and O_2 reagents (Figure 8), and lanthanum oxide and hydride species were observed as reported previously.[22,24] The same new product absorptions were observed (Table 6), but at different times in the experiment. In contrast to the H_2O_2 experiments, the **di** and HOLaO bands were strongest on deposition and **dic** and **tri** bands were very weak or not observed. Near-UV light (240−380 nm) decreased **di** and increased the **dic** and HOLaO bands, and the full arc continued this trend and produced the **tri** absorptions. Annealing to 22 K markedly increased the **tri** bands at the expense of the others. Substitution of $^{18}O_2$ shifted the bands as shown in Figure 8 and Table 7. Analogous spectra with D_2 and O_2 gave sharper **tri** bands and more separation in the two O−D stretching modes for **dic** as well as small shifts in the La−O stretching region (Figure 9). The HD reagent produced an intermediate O−D stretching band.

Calculations were also done for the analogous lanthanum species, and the structures are illustrated in Figure 10 and the frequencies are given in Tables 8−11, where they are compared with observed values.

Discussion

The new product absorptions from Y and La metal, H_2O_2, and H_2 plus O_2 reaction systems will be characterized in this investigation by isotopic shifts in both the O−H and M−O stretching modes and quantum chemical structure and frequency calculations.

Yittrium. The strongest new product absorption in the Y/water reaction system[14] at 597.9 cm^{-1} has already been assigned to $Y(OH)_2$, and our additional observations of this band at 598.0 and 598.6 cm^{-1} in hydrogen peroxide and hydrogen−oxygen experiments are in agreement. First, the **di** band shifts to 575.8 cm^{-1} with $^{18}O_2$, and the 16/18 isotopic frequency ratio 598.6/575.8 = 1.0396 is in the range expected for an antisymmetric O−Y−O stretching mode.[22] Second, the new 3773.1 cm^{-1} **di** band is associated with the 598.6 cm^{-1} band on early annealing cycles before giving way to the 3785.2 and 592.5 cm^{-1} **tri** bands on later annealing. The **di** bands are stronger with the $H_2 + O_2$ reagent, and they exhibit the same annealing behavior. The 3773.1 cm^{-1} band shifts to 3761.1 cm^{-1} with $^{18}O_2$ and to 2784.0 with $D_2 + O_2$, and the 16/18 (1.00319) and H/D (1.3553) isotopic frequency ratios are characteristic of an O−H(D) stretching mode. The observation of a doublet profile with scrambled $^{16,18}O_2$ suggests that two O atoms are involved in these vibrational modes.

The weaker 616.9 cm^{-1} band assigned by Zhou et al.[14] to $HY(OH)_2$ is observed to be stronger with $H_2 + O_2$ than with

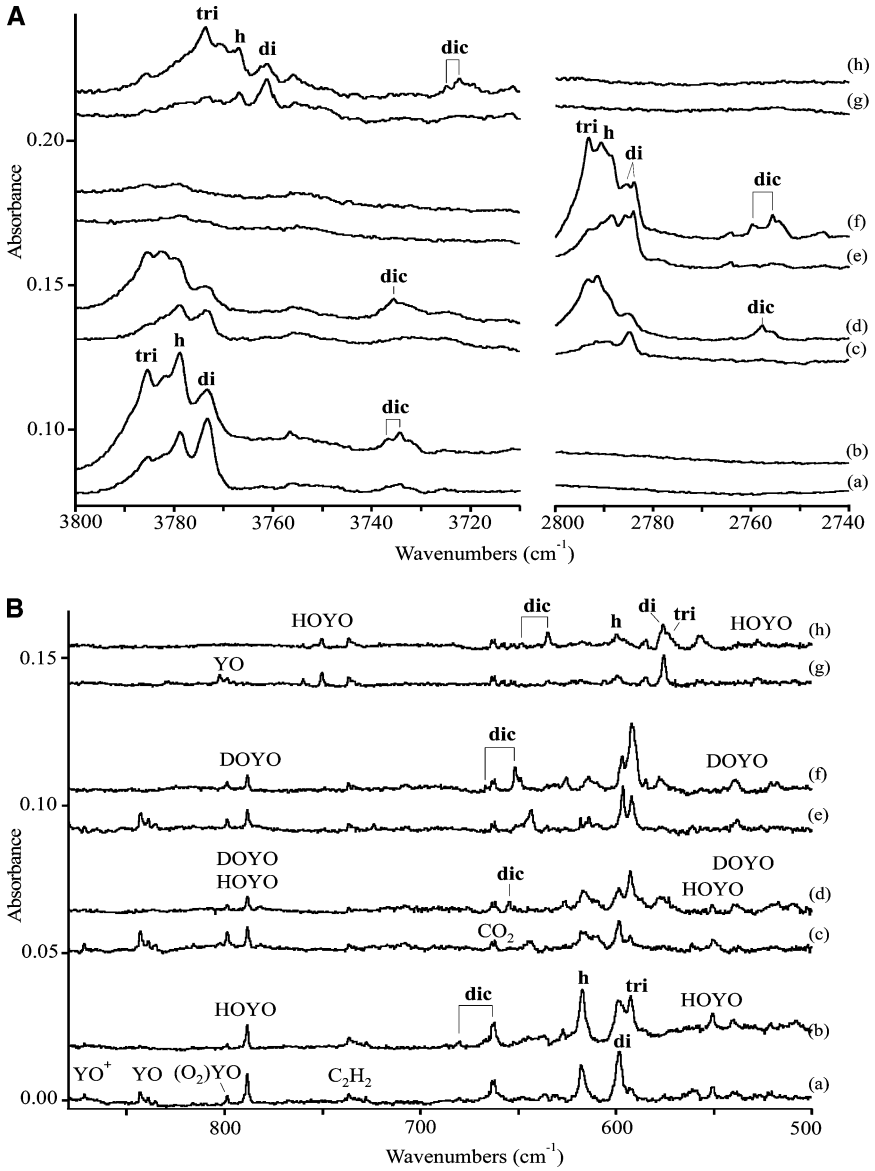

Figure 5. Infrared spectra in the O−H, O−D, and Y−O stretching regions for laser-ablated Y atom and isotopic hydrogen (6%) plus oxygen (0.4%) reaction products in excess argon at 10 K: (a) Y, H_2, and O_2 co-deposited for 60 min and (b) after full-arc (>220 nm) irradiation and annealing to 16 K; (c) Y, HD, and O_2 co-deposited for 60 min, (d) after full-arc irradiation and annealing to 16 K; (e) Y, D_2, and O_2 co-deposited for 60 min, and (f) after full-arc irradiation and annealing to 14 K; (g) Y, H_2, and $^{18}O_2$ co-deposited for 60 min, and (h) after full-arc irradiation and annealing to 18 K.

TABLE 3: Observed and Calculated Frequencies (cm^{-1}) for Y(OH)$_3$ in the C_{3h} Structure ^{1}A′ Ground State

	Y(OH)$_3$		Y(OD)$_3$		Y(^{18}OH)$_3$	
mode	obsd[a]	calcd[b]	obsd	calcd	obsd	calcd
O−H stretch		3979.2 (a′, 0)[c]		2901.5 (0)		3965.7 (0)
O−H stretch	3785.1	3978.1 (e′, 320)	2793.0	2899.4 (266)	3773.4	3964.7 (300)
Y−O stretch	592.5	611.2 (e′, 544)	577.9	597.3 (516)	570 sh	586.3 (484)
Y−O stretch		598.9 (a′$_1$, 0)		581.0 (0)		566.5 (0)
Y−O−H bend		426.9 (a″, 420)		330.6 (287)		422.8 (406)
Y−O−H bend		416.9 (e″, 0)		312.1 (0)		414.1 (0)
Y−O−H bend		273.9 (e′, 448)		207.5 (278)		272.3 (438)
Y−O−H bend		192.4 (a′, 0)		144.3 (0)		191.0 (0)
O−Y−O bend		145.8 (e′, 12)		136.6 (0)		139.2 (12)
O−Y−O bend		72.5 (a″, 19)		67.0 (15)		77.5 (18)

[a] Observed **tri** bands in solid argon. [b] Calculated at the B3LYP/6-311++G(3df,3pd)/SDD level. [c] Mode symmetry in C_{3h}, infrared intensity, km/mol, degeneracy included.

the H_2O_2 reagent (band labeled **h** in Figures 1 and 4). We also observe the Y−H stretching mode at 1368.7 cm^{-1} (not shown) and an additional associated strong band at 3778.8 cm^{-1}. The latter band shifts to 3766.8 cm^{-1} with $^{18}O_2$ (16/18 ratio 1.00316) and to 2790.6 cm^{-1} with D_2 (H/D ratio 1.3540), which characterize the strong O−H(D) stretching mode for the HY(OH)$_2$ species. Our findings support the previous identification of HY(OH)$_2$ by the Fudan group.

TABLE 4: Observed and Calculated Frequencies (cm^{-1}) for $Y(OH)_2^+$ in the C_{2v} Structure $^1A_1$ Ground State

	$Y(OH)_2$		$Y(OH)(OD)$		$Y(OD)_2$		$Y(^{18}OH)_2$		$Y(^{18}OD)_2$	
mode	obsd[a]	calcd[b]	obsd	calcd	obsd	calcd	obsd	calcd	obsd	calcd
O−H stretch	3736.8	3899.7 (a_1, 223)[c]	3735.6	3897.4 (308)	2759.6	2844.5 (142)		3886.3 (217)		2825.2 (135)
O−H stretch	3734.2	3894.9 (b_2, 393)	2757.8	2841.7 (208)	2755.5	2838.9 (272)	3722.3	3881.9 (378)	2738.3	2720.2 (254)
Y−O stretch	680.2	716.1 (a_1, 68)		714.3 (140)	667.7	695.7 (50)	648.6	682.7 (215)		667.6 (231)
Y−O stretch	662.0	712.4 (b_2, 234)	655.0	695.2 (158)	651.3	694.8 (247)	634.9	682.3 (69)	626.2	664.5 (49)
Y−O−H bend		508.6 (b_1, 338)		507.2 (177)		387.9 (215)		504.3 (330)		382.1 (207)
Y−O−H bend		505.7 (a_2, 0)		456.2 (159)		376.8 (0)		502.6 (0)		372.6 (0)
Y−O−H bend		482.6 (a_1, 154)		382.3 (100)		370.8 (101)		477.9 (147)		364.5 (97)
Y−O−H bend		410.0 (b_2, 171)		330.0 (103)		307.7 (95)		408.0 (170)		304.1 (93)
O−Y−O bend		137.6 (a_1, 4)		132.4 (3)		127.4 (2)		132.1(4)		123.4 (3)

[a] Observed **dic** bands in solid argon. [b] Calculated at the B3LYP/6-311++G(3df,3pd)/SDD level. [c] Mode symmetry in C_{2v}, infrared intensity, km/mol.

TABLE 5: Observed and Calculated Frequencies (cm^{-1}) for HOYO in the Planar $^1A'$ Ground State

	HOYO		DOYO		$H^{18}OY^{16}O$		$H^{16}OY^{18}O$		$H^{18}OY^{18}O$		$D^{18}OY^{18}O$	
mode	obsd[a]	calcd[b]	obsd	calcd	obsd	calcd	obsd	calcd	obsd	calcd	obsd	calcd
O−H stretch	3749.9	3922.5 (a′, 66)[c]	2766.5	2857.1 (52)		3909.4 (63)		3922.5 (66)		3909.4 (63)		2838.8 (47)
Y═O stretch	788.6	824.1 (a′, 226)	788.4	823.9 (226)	778.3	823.9 (229)	750.5	784.2 (206)	750.5	784.1 (209)	750.3	784.0 (209)
Y−O stretch	550.5	586.4 (a′, 130)	537.7	567.1 (167)		563.5 (108)	550.5	586.2 (129)	527.6	563.3 (108)		543.4 (150)
Y−O−H bend		470.9 (a″, 126)		355.3 (93)		467.7 (122)		470.7 (125)		467.5 (121)		350.8 (87)
Y−O−H bend		432.9 (a′, 139)		343.2 (64)		425.9 (143)		432.5 (140)		425.6 (143)		336.0 (64)
O−Y−O bend		161.1 (a′, 37)		149.7 (37)		158.8 (37)		157.1 (33)		154.6 (33)		144.5 (34)

[a] Observed **HOYO** bands in solid argon. [b] Calculated at the B3LYP/6-311++G(3df,3pd)/SDD level. [c] Mode symmetry in C_s, infrared intensity, km/mol.

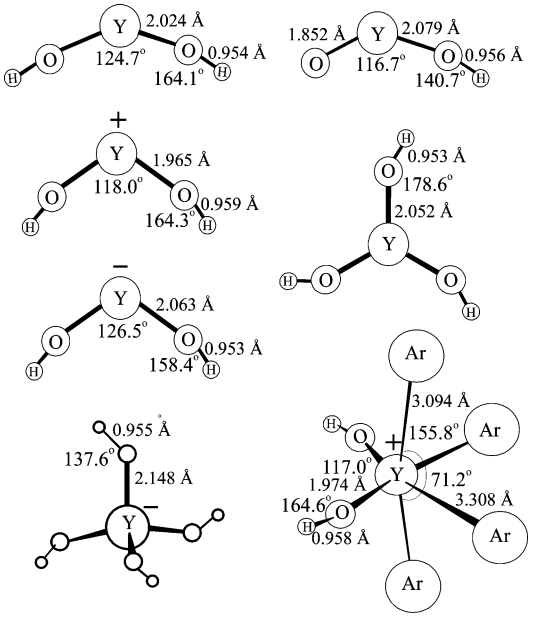

Figure 6. Structures optimized at the B3LYP/6-311++G(3df,3pd)/SDD level of theory for yittrium hydroxide species.

The 3785.2 and 592.5 cm^{-1} bands marked **tri** in yittrium experiments dominate the spectra using higher laser energy to promote more reaction, on higher temperature annealing cycles, and with higher reagent concentrations, and the highest computed O−H stretching frequency is found for $Y(OH)_3$. The 18-O shift to 3773.4 cm^{-1} and the deuterium shift to 2793.0 cm^{-1} define the isotopic frequency ratios 1.00313 and 1.3552, which again describe an O−H(D) stretching fundamental. A weak 3785.4 cm^{-1} band in the D_2O_2 experiment arises from the small amount of hydrogen in the deuterated sample, which reveals minimal coupling between O−H and O−D vibrations in the mixed isotopic product. The 592.5 cm^{-1} band shifts to 577.9 cm^{-1} with D_2 and becomes a 570 cm^{-1} shoulder on the stronger **di** band with $^{18}O_2$. A 578.0 cm^{-1} band in D_2O experiments was assigned by the Fudan group to $Y(OD)_2$, but the marked growth on this band on annealing requires its grouping with the higher $Y(OD)_3$ species. In this regard we have examined the 3700−3800 cm^{-1} region of the Y/water spectra kindly provided by Zhou, and we find a 3772.6 cm^{-1} band that tracks on annealing with the strongest 597.9 cm^{-1} absorption for $Y(OH)_2$, and a weaker 3785.1 cm^{-1} band that is associated with a weaker unassigned 597.2 cm^{-1} band that increase together on higher temperature annealing. These latter bands are assigned here to the $Y(OH)_3$ molecule.

Our B3LYP calculations using the large Gaussian basis set for H and O and SDD pseudopotential for Y obtain essentially the same structure and frequencies for $Y(OH)_2$ as found by Zhou et al. using a smaller basis set and the LANL pseudopotential.[14] It is important to note that our B3LYP calculations predict the strong O−H stretching mode for $Y(OH)_3$ to be 13 cm^{-1} above that for $Y(OH)_2$ and the strong Y−O stretching mode to be 13 cm^{-1} lower (Tables 2 and 3), and we observe them 12 cm^{-1} higher and 6 cm^{-1} lower. These frequencies are calculated higher than observed values with scale factors 0.951, 0.959 for the dihydroxide and 0.952, 0.969 for the trihydroxide, which are in the range of expected values.[37] This agreement between observed and calculated O−H and Y−O stretching frequencies, the isotopic shifts, and the production of these reactive species in three different H, O chemical systems substantiate our identification of $Y(OH)_3$, and provide further support for the identification of $Y(OH)_2$. Our calculations also predict more symmetric and antisymmetric O−D stretching mode separation (1.8 cm^{-1}) for $Y(OD)_2$, and significant infrared intensity for the symmetric mode (Table 2). These modes are partially resolved at 2785.8 and 2784.0 cm^{-1} (Figures 3 and 5) with substantial intensity for the symmetric mode, which clearly shows that the $Y(OH)_2$ molecule is bent at the metal center. In the Y(OH)(OD) case a single intermediate band is observed at 2784.9 cm^{-1} as predicted (Figure 5). This spectroscopic detail confirms the nonlinear structure (Figure 6) and the yittrium dihydroxide molecule identification.

Sharp weak new bands at 3736.8 and 3734.2 cm^{-1} increase on UV irradiation and decrease on annealing, a behavior

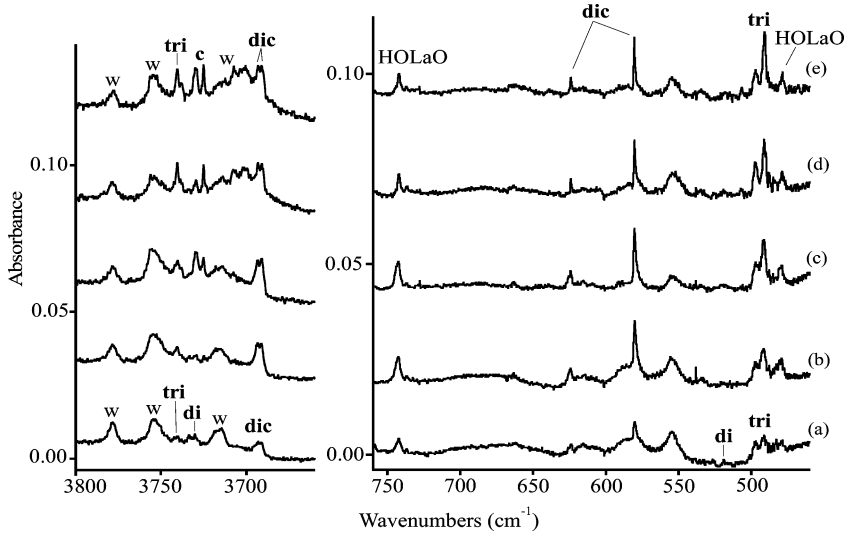

Figure 7. Infrared spectra in the O−H and La−O stretching regions for laser-ablated La atom and H_2O_2 reaction products in excess argon at 10 K: (a) La and H_2O_2 co-deposited for 60 min, (b) after 240−380 nm irradiation, (c) after >220 nm irradiation, (d) after annealing to 20 K, and (e) after a second >220 nm irradiation.

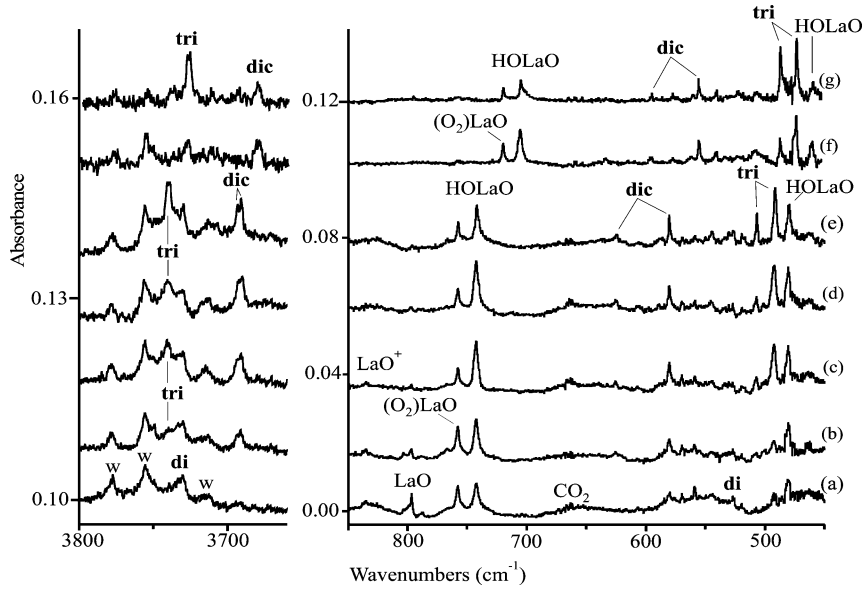

Figure 8. Infrared spectra in the O−H and La−O stretching regions for laser-ablated La atom and H_2 plus O_2 reaction products in excess argon at 10 K: (a) Y and H_2 (5%) plus O_2 (0.5%) co-deposited for 60 min, (b) after 240−380 nm irradiation, (c) after >220 nm irradiation, (d) after annealing to 18 K, and (e) after annealing to 22 K; (f) Y and H_2 (5%) plus $^{18}O_2$ (0.5%) and (g) after full-arc irradiation and annealing to 24 K.

matched by sharp new absorptions at 680.2 and 662.0 cm^{-1}. These are the only new bands that are favored relative to other product absorptions upon the addition of CCl_4 to trap ablated electrons. The YO^+ absorption is likewise favored over the YO band. Thus the four **dic** bands must be considered for a cation product.[38] This species is favored in H_2O_2 over $H_2 + O_2$ experiments and is also observed in the water investigation (weak 3735.9, 3737.6, and 662.2 cm^{-1} bands that sharpen on annealing). On the basis of the relationship to the 673.83 cm^{-1} gas-phase Y−OH fundamental, the 662.2 cm^{-1} band was assigned to YOH in solid argon.[14] However, the observed deuterium shift (11.0 cm^{-1}) is much less than the gas-phase value (18.5 cm^{-1}), which casts doubt on the YOH matrix assignment. Furthermore, the 680.2 and 662.2 cm^{-1} bands produced here with higher product yield (Figures 1−3) go together and are due to symmetric and antisymmetric Y−O stretching fundamentals (16/18 ratios 1.0487 and 1.0430) for a species with two Y−O bonds.

Our calculations predict $Y(OH)_2^+$ to have two strong O−H stretching fundamentals 65 and 70 cm^{-1} below the stronger mode for $Y(OH)_2$ and two strong Y−O stretching modes 87 and 91 cm^{-1} above the stronger Y−O mode for the neutral species. These four cation bands are observed 36 and 40 cm^{-1} below and 70 and 88 cm^{-1} above the neutral dihydroxide values, which are in reasonable agreement with calculated positions. Even more importantly, both O−H and O−D stretching modes of $Y(OH)(OD)^+$ are observed between the two modes for the pure isotopic species (Figure 5) as predicted by the calculations (Table 2). The stronger of the two Y−O stretching modes is observed, and the weaker counterpart is masked by CO_2 impurity. All of the above evidence based on four stretching modes substantiates this identification of $Y(OH)_2^+$ from the agreement of these four fundamentals and isotopic modifications with calculated values. Similar behavior was observed for $Sc(OH)_2^+$ in solid argon.[15]

TABLE 6: Mulliken Charges and Natural Electron Configurations for Group 3 Metal Hydroxide Species[a]

charge	$M(OH)_3$	$M(OH)_2$	MOH	$M(OH)_2^+$	$Ar_4M(OH)_2^+$	HMO	HOMO
q(Sc)	1.56	1.08	0.57	1.60	0.91	1.11	1.21
q(O)	−1.05	−1.05	−1.06	−0.89	−0.82	−0.64	−1.04, −0.66
q(H)	0.53	−0.51	0.49	0.59	0.59	−0.47	0.49
q(Ar)					0.17, 0.11		
q(Ar)					0.11		
NEC(Sc)[b]	$4s^{0.06}3d^{0.93}$	$4s^{0.69}3d^{0.92}$	$4s^{1.70}3d^{0.63}$	$4s^{0.03}3d^{0.89}$			
q(Y)	1.66	0.85	0.29	1.73	1.16	1.14	1.29
q(O)	−1.03	−0.90	−0.77	−0.89	−0.80	−0.69	−0.96, −0.75
q(H)	0.48	0.48	0.48	0.52	0.52	−0.45	0.42
q(Ar)					0.11, 0.10		
NEC(Y)	$5s^{0.04}4d^{0.62}$	$5s^{0.80}4d^{0.60}$	$5s^{1.84}4d^{0.36}$	$5s^{0.03}4d^{0.63}$			
q(La)	2.34	1.53	0.86	2.29	1.97	1.55	1.73
q(O)	−1.31	−1.24	−1.29	−1.18	−1.18	−1.03	−1.14, −1.03
q(H)	0.44	0.47	0.43	0.54	0.54	−0.52	0.44
q(Ar)					0.09, 0.07		
NEC(La)	$6s^{0.01}4f^{0.16}5d^{0.22}$	$6s^{0.85}4f^{0.10}5d^{0.31}$	$6s^{1.85}4f^{0.05}5d^{0.24}$	$6s^{0.01}4f^{0.14}5d^{0.29}$			

[a] Calculated at the B3LYP/6-311++G(3df,3pd)/SDD level of theory. [b] Natural electronic configuration on metal.

TABLE 7: Infrared Absorptions (cm^{-1}) for Products of the Reaction of La Atoms and H_2O_2 or $H_2 + O_2$ Molecules

$H_2O_2/H_2 + O_2$	$D_2 + O_2$	$H_2 + {}^{18}O_2$	$HD + O_2$	$D_2 + {}^{18}O_2$	identification
3740.6	2758.7	3728.1	3740.7, 2759.1	2741.7	**tri**, $La(OH)_3$
3730.3	2753.3	3718.3	3730.0	2734	**di**, $La(OH)_2$
3693.4	2725.7		3692.3	2708.6	**dic**, $La(OH)_2^+$
3691.0	2722.0	3679.9	2723.7	2705.4	**dic**, $La(OH)_2^+$
758.2	758.2	718.9	758.2	718.9	$(O_2)LaO$
624.3	610.3	593.0		582.6	**dic**, $La(OH)_2^+$
580.3	568.8	553.7	573.8	543.7	**dic**, $La(OH)_2^+$
742.5	742.2	704.7	742.2	704.4	HOLaO
519.4					**di**, $La(OH)_2$
506.6	500.9	484.4	503.9	479.8	**tri**, $La(OH)_2$
491.4	488.6	470.9		468.1	**tri**, $La(OH)_3$
480.6	470.3	457.5		449.0	HOLaO

To explain the difference between predicted and observed neutral-to-cation frequency shifts for the dihydroxide species, calculations were done for the $[Ar_4Y(OH)_2^+]$ cation complex analogous to that observed for $Sc(OH)_2^+$. The calculated tetraargon complex values [3916, 3912, 700, and 694 cm^{-1}] shift in the direction of the observed neutral-to-cation values, and show that the argon complex is a good model for $Y(OH)_2^+$ trapped in solid argon. The binding energy of four argon atoms is 16 kcal/mol, slightly lower than the 18 kcal/mol value computed for the $Sc(OH)_2^+$ complex and the ScO^+ complex in solid argon.[15,39]

The strong 788.6 cm^{-1} band is characterized by its small 0.2 cm^{-1} deuterium shift and large 38.1 cm^{-1} O-18 shift to 750.5 cm^{-1}.These bands become a doublet with scrambled isotopic oxygen, but each band is shifted inward by 0.2 cm^{-1} from the pure isotopic values as a consequence of a small amount of mixing with another mode involving an inequivalent oxygen atom. The 16/18 ratio (1.0508) is almost that for YO itself (1.0505),[22] which characterizes an almost isolated terminal Y═O stretching vibration very weakly coupled to H(D). The associated 550.5 cm^{-1} band exhibits a smaller 16/18 ratio (1.0434) and a larger 12.9 cm^{-1} deuterium shift, and these observations describe a Y−O stretching mode coupled to H(D) most likely a Y−OH(D) stretching mode. Hence, the HO−Y═O molecule is characterized. A weak 3747 cm^{-1} shoulder on the water absorption could be due to the weaker O−H stretching fundamental, but this is tentative.

Our calculations for the HOYO molecule predict a stable $^1A'$ state with strong Y−O stretching frequencies at 824.1 and 586.4 cm^{-1} and a much weaker O−H stretching mode at 3922.5 cm^{-1}. The Y═O and Y−O stretching modes are predicted 4.5% and 6.5% higher than the observed values, which is expected for the DFT calculations.[37] Agreement between the predicted and observed isotopic shifts (Table 5) confirms our identification of the HOYO molecule, which is analogous to the HOScO molecule.[15]

The YOH molecule must be produced in these experiments, but is it trapped and can we detect it by IR spectroscopy? The O−H stretching mode is calculated to be the strongest mode and to appear a few wavenumbers below $Y(OH)_2$. The weak 3762.1 cm^{-1} band (labeled **m** in Figure 1) decreases on annealing and near-UV irradiation as YOH is expected to be a very reactive species. The deuterium counterpart at 2778.5 cm^{-1} defines a 1.3540 H/D ratio. These bands are observed only with hydrogen peroxide. The weaker Y−O stretching mode should be observed just below the 673.83 cm^{-1} gas-phase value where it may be masked by carbon dioxide or stronger $Y(OH)_2^+$ absorptions. We tentatively assign the weak 3762.1 cm^{-1} absorption to the YOH intermediate species. The more stable HYO isomer is observed at 809.7 cm^{-1} as assigned by Zhou et al.[14]

The final weak band at 459 cm^{-1} in the reaction with H_2O_2 (Figure 1) decreases slightly on annealing and changes little on irradiation, and an associated 442 cm^{-1} band with D_2O_2 follows suit. These bands are weaker with lower laser energy and absent with the chlorocarbon electron trap. We believe that these bands are appropriate for the strongest absorptions of the $Y(OH)_4^-$ and $Y(OD)_4^-$ anions (observed H/D isotopic frequency ratio 1.038, calculated 1.041), and they are assigned accordingly. Recall that the YH_4^- anion is very stable[23,24] and a major product in experiments with H_2, and it is no surprise that the reaction of $Y(OH)_2^-$ with H_2O_2 is highly exothermic [179 kcal/mol] as is the analogous reaction for the isoelectronic $Zr(OH)_2$ molecule to form $Zr(OH)_4$ [199 kcal/mol exothermic].[27]

Lanthanum. The water experiments also revealed weak 3740 and 3731 cm^{-1} absorptions that tracked, respectively, with the reported 491.2 and 519.3 cm^{-1} bands on annealing and photolysis.[14] These workers assigned both lower frequency bands to $La(OH)_2$, and we agree with the latter but not with the former. Our work clearly associates the 491 and 3740 cm^{-1} bands and shows that they arise from a second product formed from the species giving rise to the first product absorbing at 519 and 3730 cm^{-1}. The 491 and 3740 cm^{-1} bands are assigned to $La(OH)_3$, and the trihydroxide molecule appears to form most readily for lanthanum. The 3740.6 cm^{-1} band shifts to 3728.1 cm^{-1} with oxygen-18 and to 2758.7 cm^{-1} with D substitution, which defines the isotopic frequency ratios 1.00335 and 1.356,

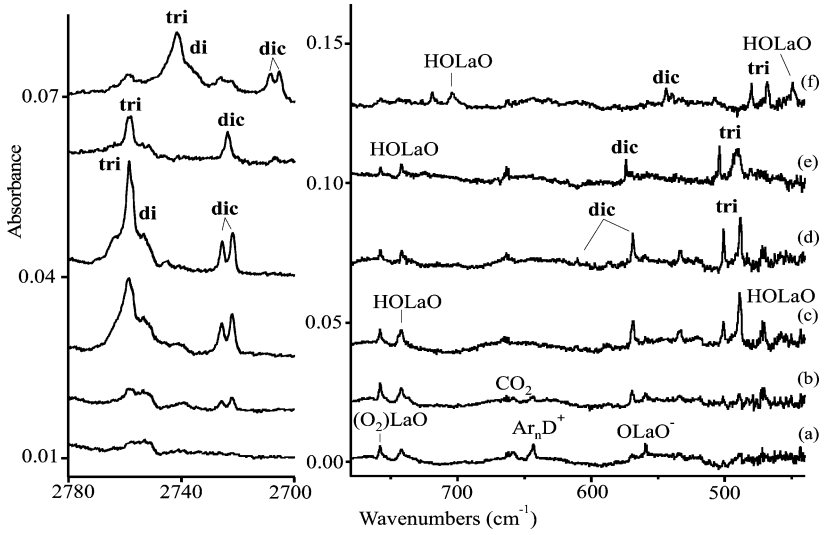

Figure 9. Infrared spectra in the O−D and Y−O stretching regions for laser-ablated Y atom and isotopic D_2 (5%) plus O_2 (0.5%) reaction products in excess argon at 10 K: (a) Y and D_2 plus O_2 co-deposited for 60 min, (b) after 240−380 nm irradiation, (c) after >220 nm irradiation, and (d) after annealing to 22 K; (e) Y and HD plus O_2 after full-arc irradiation and annealing to 20 K; (f) Y and D_2 plus $^{18}O_2$ after full-arc irradiation and annealing to 16 K.

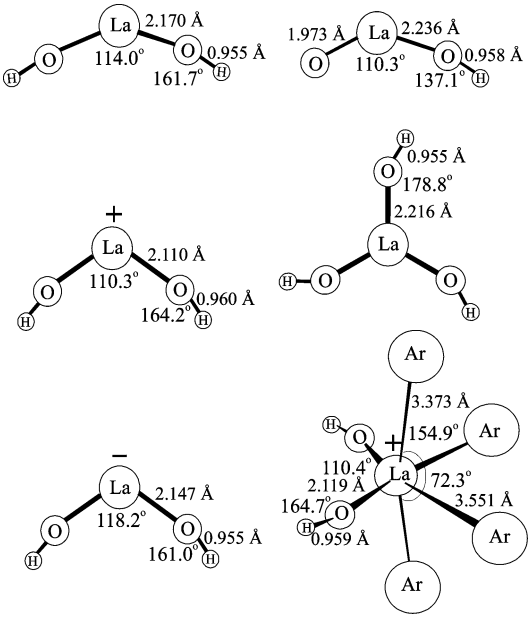

Figure 10. Structures optimized at the B3LYP/6-311++G(3df,3pd)/SDD level of theory for lanthanum hydroxide species.

respectively, for an O−H stretching mode. The 491.4 cm^{-1} band shifts to 470.9 cm^{-1} with oxygen-18 and only 3.2 cm^{-1} with D substitution and the 16/18 ratio 1.0435 is lower than the 1.0515 value for the bent LaO_2^- anion.[22] Notice that this is the dominant product after photolysis and annealing especially in La but also in Y and Sc metal experiments. The weaker 3730.3 cm^{-1} band shifts to 3718.3 cm^{-1} with oxygen-18 and to 2753.3 cm^{-1} with D substitution, and gives the 1.00323 and 1.355 isotopic frequency ratios.

Calculated frequencies are listed in Tables 8 and 9 for $La(OH)_2$ and $La(OH)_3$. Notice that the O−H stretching mode is predicted 7 cm^{-1} higher and the La−O stretching mode 21 cm^{-1} lower for the trihydroxide, and we observed these bands 10 cm^{-1} higher and 28 cm^{-1} lower. In our samples the **tri** bands are split owing to a matrix site effect or reduction in symmetry.

The four **dic** bands are produced on UV irradiation. Two O−H stretching modes are resolved at 3693.4 and 3691.0 cm^{-1} and two O−D stretching modes at 2725.2 and 2722.0 cm^{-1} (H/D ratios 1.3550 and 1.3560). The HD experiment gives intermediate bands at 3692.3 and 2723.7 cm^{-1}, which demonstrates that the original two bands are symmetric and antisymmetric stretching modes of equivalent O−H (or O−D) bonds and HD gives rise to O−H and O−D bonds. In like fashion, two La−O stretching modes are observed, a weaker band at 624.5 cm^{-1} and a stronger band at 580.4 cm^{-1}, and these bands shift to 593.0 and 553.7 cm^{-1} with oxygen-18 and define 16/18 isotopic frequency ratios of 1.0550 and 1.0479. Such ratios are characteristic of symmetric and antisymmetric La−O stretching modes in lanthanum oxide species.[22] This is confirmed in the scrambled oxygen isotopic experiment where a triplet is observed at 580.5, 562.9, and 554.0 cm^{-1} for the antisymmetric vibration of two equivalent oxygen atoms. The **dic** bands shift to 610.3 and 568.8 cm^{-1} with deuterium and an intermediate band is found at 573.8 cm^{-1} with the HD reagent where the mode symmetry is broken. The four **di** bands in the lanthanum experiments correlate with those from the yittrium studies where electron trapping showed conclusively that the **dic** absorptions are due to a positive ion.

The identification of $La(OH)_2^+$ is confirmed by comparison with the calculated frequencies in Table 10. The lowest O−H stretching frequencies and highest La−O stretching frequencies are predicted and observed for the cation species. The cation is calculated to have 55 cm^{-1} lower O−H and 74 cm^{-1} higher La−O antisymmetric stretching modes and we observe them 39 cm^{-1} lower and 61 cm^{-1} higher. Using instead the $[Ar_4La(OH)_2^+]$ complex as a model, the O−H mode is calculated 43 cm^{-1} lower and the La−O mode 62 cm^{-1} higher, which is in better agreement with experiment. We find the $La(OH)_2^+$ structure little changed in the complex, and the total binding energy of four argon atoms as 12 kcal/mol.

The tetrahydroxide anion $La(OH)_4^-$ is calculated to be very stable, but the strong frequency predicted at 438 cm^{-1} is too low for us to observe in these experiments. The reaction energies are summarized in Figure 11.

The two HOLaO bands at 742.5 and 480.6 cm^{-1} shift to 704.7 and 457.5 cm^{-1} with oxygen-18 (16/18 ratios 1.0536 and 1.0505), which are appropriate for La−O stretching modes.[22] The small deuterium shifts verify the presence of hydrogen in this species. Compared with our observations of HOScO and HOYO, the above bands are assigned accordingly. The calculated frequencies in Table 11 reveal the two strongest absorp-

TABLE 8: Observed and Calculated Frequencies (cm^{-1}) for $La(OH)_2$ in the C_{2v} Structure $^2A_1$ Ground State

	$La(OH)_2$		$La(OD)_2$		$La(^{18}OH)_2$	
mode	obsd[a]	calcd[b]	obsd	calcd	obsd	calcd
O−H stretch		3939.5 (a_1, 141)[c]		2871.1 (102)		3926.3 (135)
O−H stretch	3730.3	3938.9 (b_2, 121)	2753.5	2869.9 (98)	3718.3	3925.8 (114)
La−O stretch	519.4	575.0 (a_1, 297)		557.2 (76)		547.4 (92)
La−O stretch		546.2 (b_2, 144)		530.9 (159)		521.5 (126)
La−O−H bend		359.5 (a_1, 62)		275.6 (44)		355.9 (58)
La−O−H bend		355.6 (a_2, 0)		268.1 (88)		353.6 (0)
La−O−H bend		352.8 (b_1, 148)		264.3 (0)		349.9 (145)
La−O−H bend		286.7 (b_2, 146)		214.3 (79)		284.6 (145)
O−La−O bend		112.6 (a_1, 2)		104.7 (1)		107.8 (2)

[a] Observed **di** bands in solid argon. [b] Calculated at the B3LYP/6-311++G(3df,3pd)/SDD level. [c] Mode symmetry in C_{2v}, infrared intensity, km/mol.

TABLE 9: Observed and Calculated Frequencies (cm^{-1}) for $La(OH)_3$ in the C_{3h} Structure $^1A'$ Ground State

	$La(OH)_3$		$La(OD)_3$		$La(^{18}OH)_3$	
mode	obsd[a]	calcd[b]	obsd	calcd	obsd	calcd
O−H stretch		3946.5 (a′, 0)[c]		2876.4 (0)		3933.2 (0)
O−H stretch	3740.6	3946.3 (e′, 224)	2758.7	2899.4 (206)	3728.1	3933.1 (208)
La−O stretch	491.4	611.2 (a′, 0)	488.6	531.9 (0)	470.9	518.4 (0)
La−O stretch		524.9 (e′, 526)		512.1 (520)		501.5 (480)
La−O−H bend		434.6 (a″, 467)		334.3 (311)		430.4 (451)
La−O−H bend		422.4 (e″, 0)		315.8 (0)		419.7 (0)
La−O−H bend		300.5 (e′, 466)		223.8 (282)		299.0 (456)
La−O−H bend		196.4 (a′, 0)		146.9 (0)		195.1 (0)
O−La−O bend		124.3 (e′, 16)		118.5 (6)		118.4 (16)
O−La−O bend		27.6 (a″, 19)		25.5 (16)		26.6 (17)

[a] Observed **tri** bands in solid argon. [b] Calculated at the B3LYP/6-311++G(3df,3pd)/SDD level. [c] Mode symmetry in C_{3h}, infrared intensity, km/mol, degeneracy included.

TABLE 10: Observed and Calculated Frequencies (cm^{-1}) for $La(OH)_2^+$ in the C_{2v} Structure $^1A_1$ Ground State

	$La(OH)_2$		La(OH)(OD)		$La(OD)_2$		$La(^{18}OH)_2$		$La(^{18}OD)_2$	
mode	obsd[a]	calcd[b]	obsd	calcd	obsd	calcd	obsd	calcd	obsd	calcd
O−H stretch	3693.4	3887.7 (a_1, 235)[c]	3692.3	3885.9 (270)	2725.7	2834.4 (155)		3874.5 (227)	2708.6	2815.5 (146)
O−H stretch	3691.0	3884.3 (b_2, 305)	2723.7	2832.3 (186)	2722.0	2830.3 (217)	3679.9	3871.3 (292)	2705.4	2811.8 (202)
La−O stretch	624.3	650.0 (a_1, 92)		642.7 (89)		630.4 (67)	593.0	618.8 (92)		601.3 (65)
La−O stretch	580.3	619.7 (b_2, 207)	573.8	609.1 (202)	568.8	603.5 (220)	553.7	591.2 (185)	543.7	577.3 (203)
La−O−H bend		489.5 (b_1, 367)		483.8 (200)		370.4 (227)		485.7 (358)		365.3 (218)
La−O−H bend		477.3 (a_2, 0)		414.9 (152)		354.4 (0)		474.5 (0)		350.8 (0)
La−O−H bend		443.4 (a_1, 140)		362.0 (97)		340.7 (93)		438.9 (133)		334.8 (89)
La−O−H bend		359.5 (b_2, 187)		291.0 (112)		269.5 (104)		356.9 (186)		266.2 (101)
O−La−O bend		142.4 (a_1, 2)		137.0 (2)		131.9 (1)		136.3(2)		127.3 (1)

[a] Observed **dic** bands in solid argon. [b] Calculated at the B3LYP/6-311++G(3df,3pd)/SDD level. [c] Mode symmetry in C_{2v}, infrared intensity, km/mol.

TABLE 11: Observed and Calculated Frequencies (cm^{-1}) for HOLaO in the Planar $^1A'$ Ground State

	HOLaO		DOLaO		$H^{18}OLa^{18}O$		$D^{18}OLa^{18}O$	
mode	obsd[a]	calcd[b]	obsd	calcd	obsd	calcd	obsd	calcd
O−H stretch		3899.6 (a′, 56)[c]		2839.9 (46)		3886.7 (53)		2821.9 (41)
La═O stretch	742.5	749.6 (a′, 211)	742.2	749.5 (210)	704.7	711.2 (193)	704.4	710.9 (191)
La−O stretch	480.6	514.1 (a′, 123)	470.9	497.1 (172)	457.5	493.5 (93)	449.0	474.5 (153)
La−O−H bend		457.6 (a″, 133)		342.3 (93)		454.6 (128)		338.4(88)
La−O−H bend		421.1 (a′, 133)		327.9 (53)		413.8 (144)		322.3 (54)
O−La−O bend		133.4 (a′, 28)		123.7 (28)		127.6 (25)		119.3 (25)

[a] Observed **HOLaO** bands in solid argon. [b] Calculated at the B3LYP/6-311++G(3df,3pd)/SDD level. [c] Mode symmetry in C_s, infrared intensity, km/mol.

tions to be the La═O and La−O stretching modes at 749.6 and 514.1 cm^{-1}, which are 1.0% and 7.0% higher than the observed values and in good enough agreement to substantiate this assignment.

Group 3 Trends. The diagnostic O−H stretching frequencies for the trihydroxides are 10−12 cm^{-1} higher than those of the dihydroxides, and both decrease on going down the Group 3 family, as found for the Group 2, 4, and 12 dihydroxide molecules.[26−28] This decrease is not observed for the $M(OH)_2^+$ cations, where $Y(OH)_2^+$ appears above $Sc(OH)_2^+$. Although the metal atoms have a common $(n-1)$d ns^2 valence electron configuration, the metal cations are different in this regard [3d 4s, $5s^2$, and $5d^2$, respectively].[40] It therefore appears that $Y(OH)_2^+$ is out of line because Y^+ with two s electrons binds two OH radicals less effectively and does less electron withdrawing from the OH bonds. Notice in Table 6 that the Mulliken charge increases on going down the family group for a particular hydroxide, as expected from the decrease in

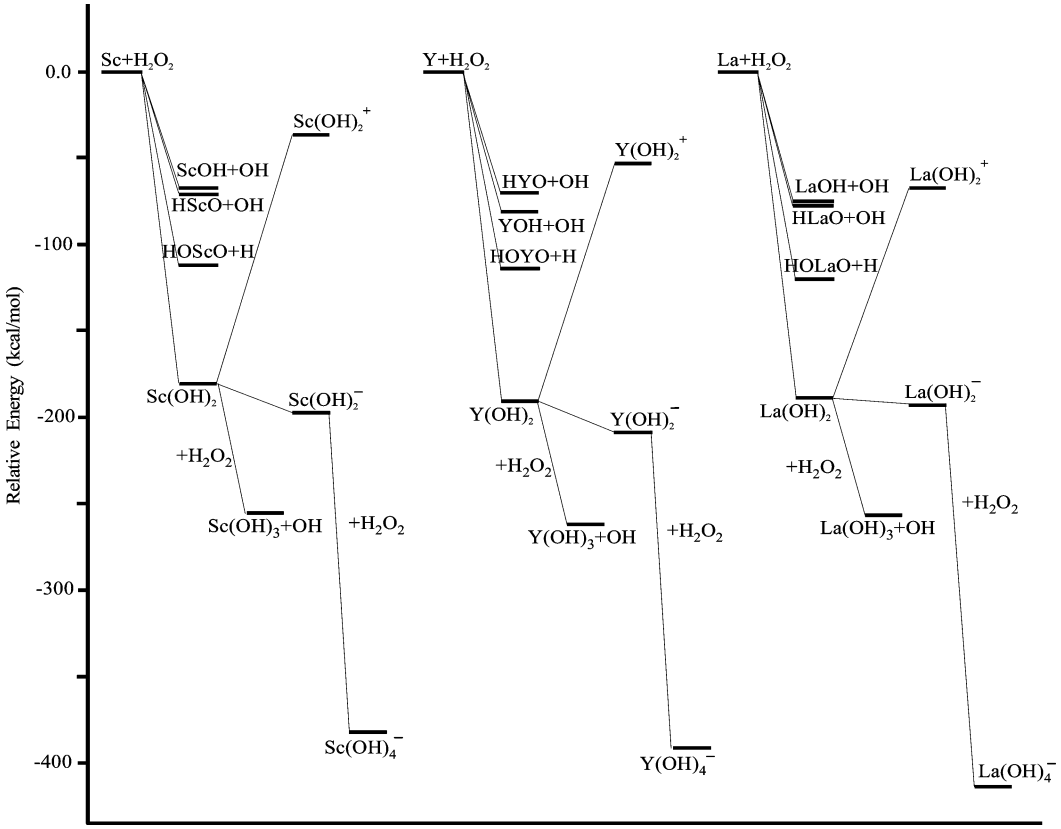

Figure 11. Relative energies of Group 3 metal hydroxide reaction products.

ionization energy, and decreases with decreasing number of OH groups in the hydroxide for all of the metals. The HOMO molecules are special being both oxide and hydroxide, and their Mulliken charges fall between the trihydroxide and dihydroxide values. Finally, the Mulliken charges on the metal centers increase when one, two, and three OH ligands are bonded to the metal center as progressively more electron density from the metal is involved in forming σ bonds to the OH ligands.

Another interesting comparison is found in the natural electron configurations[41] for the metal centers, which are summarized in Table 6. For the linear monohydroxide molecules, the s orbital occupancy is 1.70 to 1.85. In the dihydroxide molecules for Sc the configuration is $4s^{0.69}\ 3d^{0.92}$, for Y $5s^{0.80}\ 4d^{0.60}$, and for La $6s^{0.85}\ 4f^{0.10}\ 5d^{0.0.31}$. Notice that the s character increases and the d character decreases on going down the Group 3 family of dihydroxides and the valence angle at the metal center decreases from 130.0° to 124.7° to 114.0°, which is consistent with more sd character in the metal−OH ligand bonding. For the dihydroxide cations the valence s orbital occupancy is very low, but the valence d orbital occupancy decreases in like manner as the valence angle decreases from 119.8° to 118.0° to 110.3°. In the trihydroxides for Sc the natural electron configuration is $4s^{0.06}\ 3d^{0.93}$, for Y $5s^{0.04}\ 4d^{0.62}$, and for La $6s^{0.01}\ 4f^{0.16}\ 5d^{0.22}$. These trends show that more s electron density is involved in the bonding to successively more OH ligands.

Reaction Mechanisms. All of our metal atom reactions with H_2O_2 form the metal dihydroxide molecules by direct insertion,[15,26−28] and reaction 1 is computed at the B3LYP level to be exothermic [181, 190, and 188 kcal/mol, respectively, for M = Sc, Y, and La]. The trihydroxide molecule is produced by secondary reaction 2, which is exothermic [75, 71, and 66 kcal/mol for M = Sc, Y, and La, respectively] and is suggested by the decrease in **di** and increase in **tri** absorptions on sample irradiation. The $M(OH)_3$ molecules are stable to dehydration, which is a process endothermic by 74, 79, and 66 kcal/mol, respectively, for the Group 3 metals. Another possible reaction 4 with the monohydroxide is also favorable [182 kcal/mol exothermic for Y]. The HOMO molecules are probably formed through decomposition of the energized product of reaction 1 as suggested in the relative energy diagram shown in Figure 11.

$$M + H_2O_2 \rightarrow M(OH)_2 \quad (1)$$

$$M(OH)_2 + H_2O_2 \rightarrow M(OH)_3 + OH \quad (2)$$

$$M(OH)_3 \rightarrow HOMO + HOH \quad (3)$$

$$YOH + H_2O_2 \rightarrow Y(OH)_3 \quad (4)$$

The dihydroxide cations are formed here in the initial reaction with laser-ablated M^+ cations, as attested by the observation of YO^+ and $Y^{18}O^+$ in these experiments, and by photoionization of the neutral dihydroxide, reactions 5 and 6. The ionization energies computed for the dihydroxide molecules are 143, 136, and 123 kcal/mol, respectively.

$$M^+ + H_2O_2 \rightarrow M(OH)_2^+ \quad (5)$$

$$M(OH)_2 + UV \rightarrow M(OH)_2^+ + e^- \quad (6)$$

Reaction 6 proceeds with 240−380 nm irradiation to give about half of the cation yield as >220 nm irradiation for La, only 20% as much for Y, but only >220 nm irradiation formed the cation for Sc,[15] which is in line with the computed ionization energies and the need for a slight red matrix shift for the photoionization process owing to the formation of $Ar_4\ M(OH)_2^+$ cation complexes.

The $M(OH)_2^-$ anions are computed to be stable but without strong IR absorptions; however, the stable $Y(OH)_4^-$ anion has a very strong degenerate Y−O stretching mode that is observed here at 459 cm^{-1} from the exothermic [179 kcal/mol] reaction 7.

$$Y(OH)_2^- + H_2O_2 \rightarrow Y(OH)_4^- \quad (7)$$

Conclusions

Yittrium and lanthanum atoms react with H_2O_2 to form the $M(OH)_2$ and $M(OH)_3$ molecules and the HOMO dehydration products. The $M(OH)_2$ molecules appear to react readily with more H_2O_2 to form the valence-saturated trihydroxide molecules. Both symmetric and antisymmetric O−D stretching modes were observed for the $M(OD)_2$ molecule, which shows that these dihydroxide molecules are bent at the metal centers. The $M(OH)_2^+$ cations are formed and trapped in solid argon as argon complexes. These cations are characterized by the observation of symmetric and antisymmetric O−H and M−O stretching modes. The cation O−H stretching frequencies are lower than those for the neutral $M(OH)_2$ molecules, which is due to electron density withdrawal in bonding to the cation center and O−H bond lengthening as found by B3LYP calculations.

Acknowledgment. We gratefully acknowledge financial support for this work from NSF Grant CHE 03-52487 and the opportunity to examine unpublished spectra from the work reported in ref 14 courtesy of M. Zhou.

References and Notes

(1) Schubert, K.; Seitz, A. *Z. Anorg. Chem.* **1948**, *256*, 226.
(2) Schubert, K.; Seitz, A. *Z. Anorg. Chem.* **1947**, *254*, 254.
(3) Christensen, A. N.; Hazell, R. G.; Nilsson, A *Acta. Chem. Scand.* **1967**, *21*, 481.
(4) Zachariasen, W. H. *Acta Crystallogr*. **1948**, *1*, 265. Zachariasen, W. H. *J. Chem. Phys.* **1948**, *16*, 254.
(5) Atoji, M.; Williams, D. E. *J. Chem. Phys.* **1959**, *31*, 329.
(6) Wells, A. F. *Structural Inorganic Chemistry*, 4th ed.; Clarendon Press, Oxford, UK, 1975.
(7) Cotton, F. A.; Wilkinson, G.; Murillo, C. A.; Bochmann, M. *Advanced Inorganic Chemistry*, 6th ed.; Wiley: New York, 1999.
(8) Wang, X.; Andrews, L. *Inorg. Chem.* **2005**, *44*, 7189.
(9) McWhan, D. B.; Lundgren, G. *Inorg. Chem.* **1966**, *5*, 284
(10) Hansson, M. *Acta Chem. Scand.* **1969**, *23*, 3541
(11) Adam, A. G.; Athanassenas, K.; Gillett, D. A.; Kingston, C. T.; Merer, A. J.; Peers, J. R. D.; Rixon, S. J. *J. Mol. Spectrosc.* **1999**, *45*, 196.
(12) Kaufman, J. W.; Hauge, R. H.; Margrave, J. L. *J. Phys. Chem.* **1985**, *89*, 3547.
(13) Zhang, L.; Dong, J.; Zhou, M. F. *J. Phys. Chem. A* **2000**, *104*, 8882.
(14) Zhang, L.; Shao, L.; Zhou, M. *Chem. Phys.* **2001**, *272*, 27.
(15) Wang, X.; Andrews, L. *J. Phys. Chem. A* **2006**, *110*, 1850 (Sc + H_2O_2).
(16) Clemmer, D. E.; Aristov, N.; Armentrout, P. B. *J. Phys. Chem.* **1993**, *97*, 544.
(17) Magnera, T. F.; David, D. E.; Michl, J. *J. Am. Chem. Soc.* **1989**, *111*, 4100.
(18) Crellin, K. C.; Beauchamp, J. L.; Goddard, W. A.; Geribaldi, S.; Decouzon, M. *Int. J. Mass Spectrom.* **1999**, *183*, 121.
(19) Bauschlicher, C. W., Jr.; Partridge, H. *Chem. Phys. Lett*. **1997**, *272*, 127.
(20) Ricca, A.; Bauschlicher, C. W., Jr. *J. Phys. Chem. A* **1997**, *101*, 8949.
(21) Bauschlicher, C. W., Jr.; Zhou, M. F.; Andrews, L.; Tobias Johnson, J. R.; Panas, I.; Snis, A.; Roos, B. *J. Phys. Chem. A* **1999**, *103*, 5463.
(22) Andrews, L.; Zhou, M. F.; Chertihin, G. V.; Bauschlicher, C. W., Jr. *J. Phys. Chem. A* **1999**, *103*, 6525.
(23) Wang, X.; Andrews, L. *J. Am. Chem. Soc.* **2002**, *124*, 7610.
(24) Wang, X.; Chertihin, G. V.; Andrews, L. *J. Phys. Chem. A* **2002**, *106*, 9213.
(25) Andrews, L. *Chem. Soc. Rev*. **2004**, *33*, 123 and references therein.
(26) Wang, X.; Andrews, L. *J. Phys. Chem. A* **2005**, *109*, 2782.
(27) Wang, X.; Andrews, L. *J. Phys. Chem. A* **2005**, *109*, 3847.
(28) Wang, X.; Andrews, L. *J. Phys. Chem. A* **2005**, *109*, 10689.
(29) Pettersson, M.; Tuominen, S.; Rasanen, M. *J. Phys. Chem. A* **1997**, *101*, 1166.
(30) Pehkonen, S.; Pettersson, M.; Lundell, J.; Khriachtchev, L.; Rasanen, M. *J. Phys. Chem. A* **1998**, *102*, 7643.
(31) Frisch, M. J.; Trucks, G. W.; Schlegel, H. B.; Scuseria, G. E.; Robb, M. A.; Cheeseman, J. R.; Zakrzewski, V. G.; Montgomery, J. A., Jr.; Stratmann, R. E.; Burant, J. C.; Dapprich, S.; Millam, J. M.; Daniels, A. D.; Kudin, K. N.; Strain, M. C.; Farkas, O.; Tomasi, J.; Barone, V.; Cossi, M.; Cammi, R.; Mennucci, B.; Pomelli, C.; Adamo, C.; Clifford, S.; Ochterski, J.; Petersson, G. A.; Ayala, P. Y.; Cui, Q.; Morokuma, K.; Malick, D. K.; Rabuck, A. D.; Raghavachari, K.; Foresman, J. B.; Cioslowski, J.; Ortiz, J. V.; Stefanov, B. B.; Liu, G.; Liashenko, A.; Piskorz, P.; Komaromi, I.; Gomperts, R.; Martin, R. L.; Fox, D. J.; Keith, T.; Al-Laham, M. A.; Peng, C. Y.; Nanayakkara, A.; Gonzalez, C.; Challacombe, M.; Gill, P. M. W.; Johnson, B.; Chen, W.; Wong, M. W.; Andres, J. L.; Gonzalez, C.; Head-Gordon, M.; Replogle, E. S.; Pople, J. A. *Gaussian 98*, Revision A.6; Gaussian, Inc.: Pittsburgh PA, 1998 and references therein.
(32) Frisch, M. J.; Pople, J. A.; Binkley, J. S. *J. Chem. Phys.* **1984**, *80*, 3265.
(33) Andrae, D.; Haeussermann, U.; Dolg, M.; Stoll, H.; Preuss, H. *Theor. Chim. Acta* **1990**, *7*, 123.
(34) (a) Langford, V. S.; McKinley, A. J.; Quickenden, T. I. *J. Am. Chem. Soc.* **2000**, *122*, 12859. (b) Cooper, P. D.; Kjaergaard, H. G.; Langford, V. S.; McKinley, A. J.; Quickenden, T. I.; Schofield, D. P. *J. Am. Chem. Soc.* **2003**, *125*, 6048.
(35) (a) Milligan, D. E.; Jacox, M. E. *J. Chem. Phys.* **1963**, *38*, 2627. (b) Smith, D. W.; Andrews, L. *J. Chem. Phys.* **1974**, *60*, 81.
(36) Cheng, B.-M.; Lee, Y.-P.; Ogilvie, J. F. *Chem. Phys. Lett.* **1988**, *109*, 151.
(37) Scott, A. P.; Radom, L. *J. Phys. Chem.* **1996**, *100*, 16502.
(38) Andrews, L.; Citra, A. *Chem. Rev*. **2002**, *102*, 885 and references therein.
(39) Zhao, Y.; Wang, G.; Chen, M.; Zhou, M. F. *J. Phys. Chem. A* **2005**, *109*, 6621.
(40) Moore, C. E. *Atomic Energy Levels*; National Bureau of Standards, Circular 467; National Bureau of Standards: Washington, D.C., 1952.
(41) Reed, A. J.; Curtiss, L. A.; Weinhold, F. *Chem. Rev.* **1988**, *88*, 899.